Available online at www.sciencedirect.com
SCIENCE DIRECT®
Journal of Catalysis 239 (2006) 347–353
JOURNAL OF CATALYSIS
www.elsevier.com/locate/jcat

Ziegler–Natta catalysts for propylene polymerization: Morphology and crystal structure of a fourth-generation catalyst

Main Chang [a,*], Xinsheng Liu [b], Patricia J. Nelson [b], George R. Munzing [b], Thomas A. Gegan [b], Yury V. Kissin [b,*,1]

[a] *Engelhard Corporation, 10001 Chemical Road, Pasadena, TX 77507, USA*
[b] *Engelhard Corporation, Research Center, 101 Wood Avenue, Iselin, NJ 08830, USA*

Received 19 December 2005; revised 13 February 2006; accepted 14 February 2006
Available online 20 March 2006

Abstract

The article presents a detailed morphological study of a $TiCl_4/MgCl_2$ Ziegler–Natta catalyst for isospecific polymerization of propylene. A combination of SEM, TEM, and XRD data demonstrates that the catalyst exhibits a unique "sea urchin"-type crystallite structure. The body of each primary catalyst particle, a sphere 5–8 μm in diameter, is tightly filled with long crystal rods of $MgCl_2$. The rods radiate from the center of the primary particles. The lengths of the rods are quite large and, at a maximum, can reach the length of the radius of the primary particles. Within each rod, the planes of the Cl–Mg–Cl layers are oriented mostly perpendicularly to the lengths of the rods. This arrangement of $MgCl_2$ crystals in the rods exposes their lateral surfaces, the surfaces where the active sites of Ziegler–Natta catalysts are subsequently formed after treatment of the support particles with $TiCl_4$.

Keywords: Ziegler–Natta catalyst; Crystal structure of; Morphology of; Propylene polymerization

1. Introduction

Titanium-based Ziegler–Natta catalysts of the fourth generation for isospecific propylene polymerization contain $TiCl_4$, $MgCl_2$ as a support, and alkyl esters of aromatic diacids as modifying organic components of solid catalysts. In general, these solid components are prepared by fashioning highly porous particles of anhydrous $MgCl_2$ with controlled morphology. Several different techniques can be used to manufacture of $MgCl_2$ particles suitable for catalyst preparation [1], including (a) recrystallization of $MgCl_2$ from a mixture of ethanol, methyl siloxane oil, and paraffin oil at low temperature [2]; (b) precipitation of complexes of $MgCl_2$ from solutions in alcohols or other polar solvents, followed by thermal or chemical decomposition of the complexes with the formation of microcrystalline $MgCl_2$ [3]; and (c) chemical synthesis of $MgCl_2$ from dialkylmagnesium compounds or Grignard reagents, by reacting them with chloro-containing compounds such as HCl, alkyl chlorides, $SiCl_4$, and $TiCl_4$ [4]. After the $MgCl_2$ particles are formed, dialkyl phthalates and $TiCl_4$ are deposited on the surface of the $MgCl_2$ crystallites.

These solid catalysts are activated in polymerization reactions with combinations of $AlEt_3$ and alkylalkoxy or arylalkoxysilanes $R_xSi(OR')_{4-x}$. The molar [Al]:[Si] ratio in the cocatalyst mixtures varies from 10:1 to 20:1, and the molar [Al]:[Ti] ratio in the final catalyst systems is ∼250 [5–9]. A number of authors have described morphological, chemical, and spectroscopic analysis of solid components of such catalysts, as well as various model systems [10–13]. In most cases, the particles of these catalysts are composed of loosely agglomerated small $MgCl_2$ crystallites.

This paper presents a detailed morphological study of a fourth-generation Ziegler–Natta catalyst manufactured by Engelhard Corporation under the trade name Lynx® 1000. The catalyst exhibits a unique "sea urchin"-type crystallite struc-

* Corresponding authors.
E-mail addresses: main.chang@engelhard.com (M. Chang), ykissin@rutchem.rutgers.edu (Y.V. Kissin).
[1] Permanent address: Department of Chemistry and Chemical Biology, Rutgers, The State University of New Jersey, 610 Taylor Road, Piscataway, NJ, 08854, USA.

0021-9517/$ – see front matter
doi:10.1016/j.jcat.2006.02.009

ture characterized by two features: rod-like $MgCl_2$ crystallites elongated in the direction of the *c* axis and tight packing of the crystallites within the catalyst particles. The crystallites elongated in the *c* axis direction have a high lateral surface area, which results in the formation of a highly active catalyst affording productivity of ∼40 kg of polypropylene/(g of catalyst h). Tight packing of the $MgCl_2$ crystallites within the primary catalyst particles results in the synthesis of polypropylene with high bulk density, 0.44–0.48 g/cc [14,15].

2. Experimental

2.1. Solid catalyst

The catalyst was synthesized as described previously [16]. Microcrystalline particles of $MgCl_2$ are prepared by dissolving a mixture of complexes of anhydrous $MgCl_2$ with epichlorohydrin and tributyl phosphate in toluene at 50 °C, cooling the solution to −25 °C, and removing the organic components from the $MgCl_2$ complexes with excess of $TiCl_4$. Heating this solution to 80 °C results in precipitation of solid support particles in a microspherical form. The support is contacted with diisobutyl phthalate, activated with $TiCl_4$ in toluene solution at an increased temperature, and finally washed thoroughly with a series of aliphatic and aromatic solvents. The catalyst composition was as follows: [Ti] ∼1.9 wt%, [Mg] ∼18 wt%, [Cl] ∼56 wt%, [phthalate] ∼13 wt%. In general terms, the catalyst can be viewed as $MgCl_2$ in a microcrystalline form containing Ti species, at [Ti]:[Mg] = 0.055, and the phthalate species, at [phthalate]:[Mg] = 0.27, on the surface of the $MgCl_2$ crystallites.

2.2. Scanning electron microscopy

The secondary electronic image analysis was conducted on a JEOL 6500 Schottky thermal field emission scanning electron microscope at 3–5 kV and 10-mm working distance. The energy-dispersive spectroscopic analysis of X-ray (EDS) was conducted at 15 kV on a PGT SPIRIT workstation equipped with a 50-mm^2 light element germanium detector. To preserve the morphology of the catalyst in the course of the analysis and also observe morphological details of the catalyst particles, the following procedure was adopted to sample the catalyst for SEM analysis. In a nitrogen box, the catalyst powder was placed on a glue-covered tape (PETE tape or copper) attached to a sample holder. To avoid charging of catalyst particles, most of the glue was removed from the tape surface. A part of the catalyst sheet attached to the tape was fractured with a thin blade. This technique produces a large number of catalyst particles cut to different degrees, including some particles cut in halves, with their cross-sections facing upward. The sample holder with the catalyst was very quickly (within 1 s) transferred from a nitrogen-filled plastic jar into the loading chamber of the microscope filled with nitrogen. Subsequent elemental analysis demonstrated that the catalyst particles retained their shape and microstructure and that the oxygen uptake by the catalyst was minimal.

2.3. Transmission electron microscopy

TEM images were produced with a JEOL 2011 200 kV transmission electron microscope. In a nitrogen box, a small quantity of ground catalyst powder was placed onto a supporting grid (200 mesh) and transferred to the microscope using a GATAN environmental holder.

2.4. X-Ray diffraction measurement

XRD patterns were collected on a PW 3020 diffractometer. In a nitrogen box, an 11 × 13 mm aluminum holder, 2 mm deep, was filled with dry catalyst powder, and the opening of the holder was tightly covered with thin polypropylene film.

3. Results and discussion

3.1. Catalyst morphology

SEM microphotographs of the catalyst at a low magnification (600×) show that the catalyst particles have a spheroid shape without sharp edges and range in diameter from 15 to 25 μm. Observations at a higher magnification (5000–5500×; Fig. 1) show that the catalyst particles are agglomerates of several spherical primary particles, each 5–8 μm in diameter. The catalyst particles contain from 5 to more than 20 primary particles. The primary particles within each catalyst particle are tightly fused, and only 30–50% of their surfaces are exposed.

SEM observations at magnifications of 10,000–40,000× provide information on the morphology of the primary particles. The surfaces of the primary particles have a grainy texture and many thin cracks. Examination of the cracks shows that the surface grains are the tips of rod-like (columnar) structures that expand from the centers of the primary particles to their surfaces (Fig. 2). The diameters of the rod-like formations range from ∼50 to ∼120 nm. In some cases, the rods branch en route from the centers of the primary particles to their surfaces.

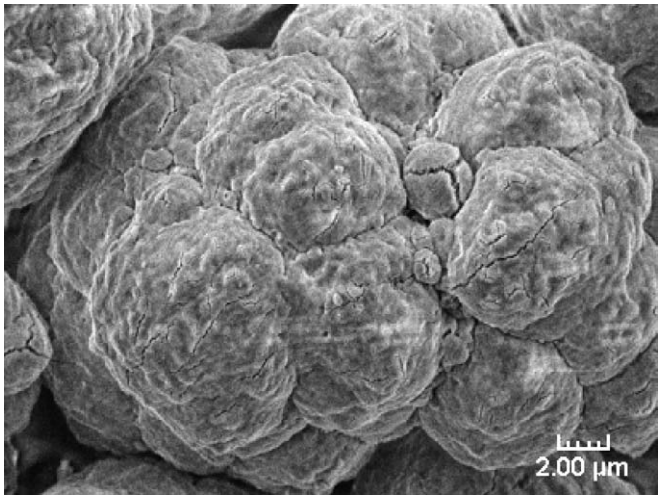

Fig. 1. SEM photograph of a catalyst particle, collected at magnification 5000×.

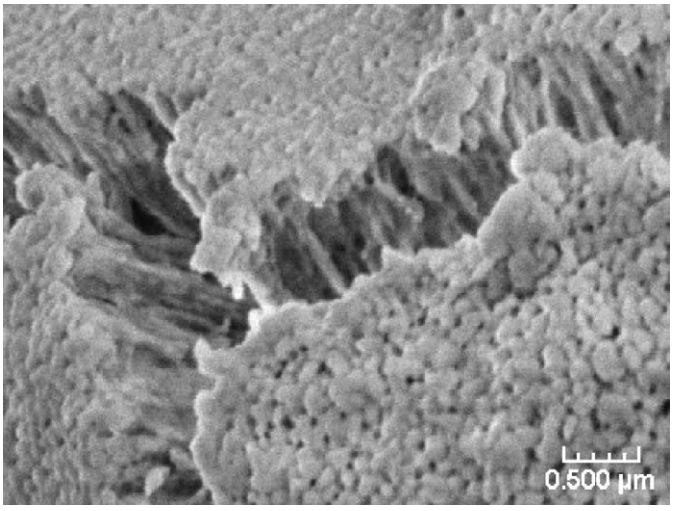

Fig. 2. SEM photograph of the surface of a primary catalyst particle, collected at magnification 15,000×.

Gentle grinding the catalyst particles in a mortar or shearing a bed of catalyst particles with a sharp blade results in fragmentation of the catalyst particles into primary particles and, in some cases, breaking up of the primary particles. Fig. 3 shows two such partially broken primary particles. The crystalline rods occupy all of the volume of the primary particles. Rods up to 2000 nm long can be directly observed. Overall, the morphology of the catalyst particles is completely different from the morphology of anhydrous $MgCl_2$ that crystallizes in a form of relatively thin platelets.

Two photographs of cross-sections of the primary catalyst particles are shown in Fig. 4. The whole volume of each primary particle is tightly packed with the crystalline rods. The gaps between the rods are small (2–5 nm). Apparently, these gaps account for the high surface area of the catalyst. The rods are not connected to one another at their sides. Cutting the catalyst particles with a blade often causes peeling off of particle fragments due to poor lateral cohesion of the rods (Fig. 4A).

This catalyst morphology (Figs. 3 and 4), reminiscent of the sea urchin body layout, is different from usual morphol-

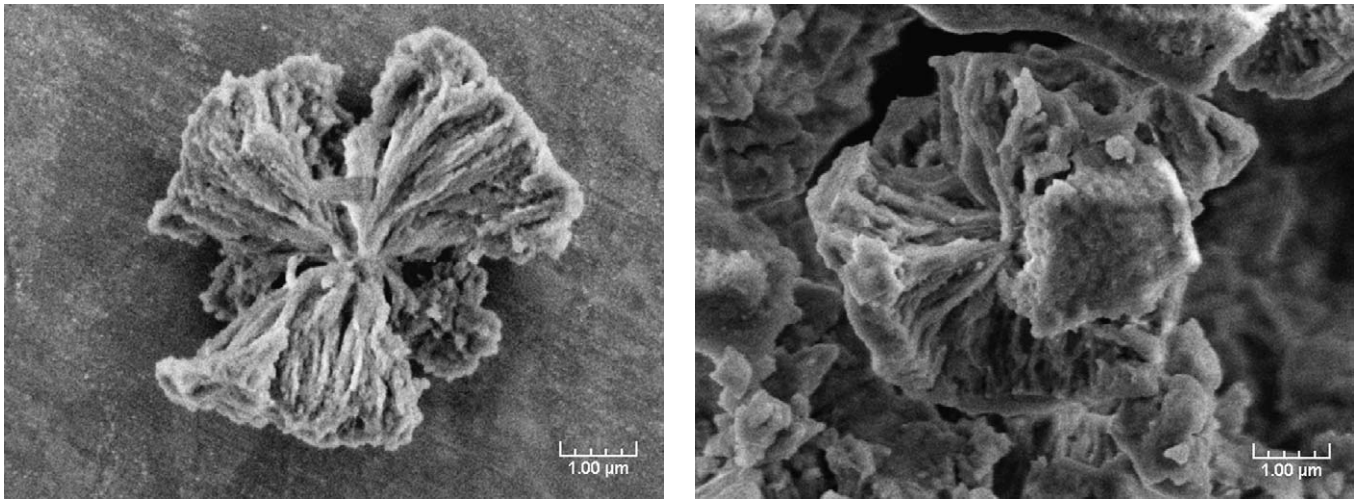

Fig. 3. SEM photographs of broken primary catalyst particles with exposed crystalline rods, collected at magnification 15,000×.

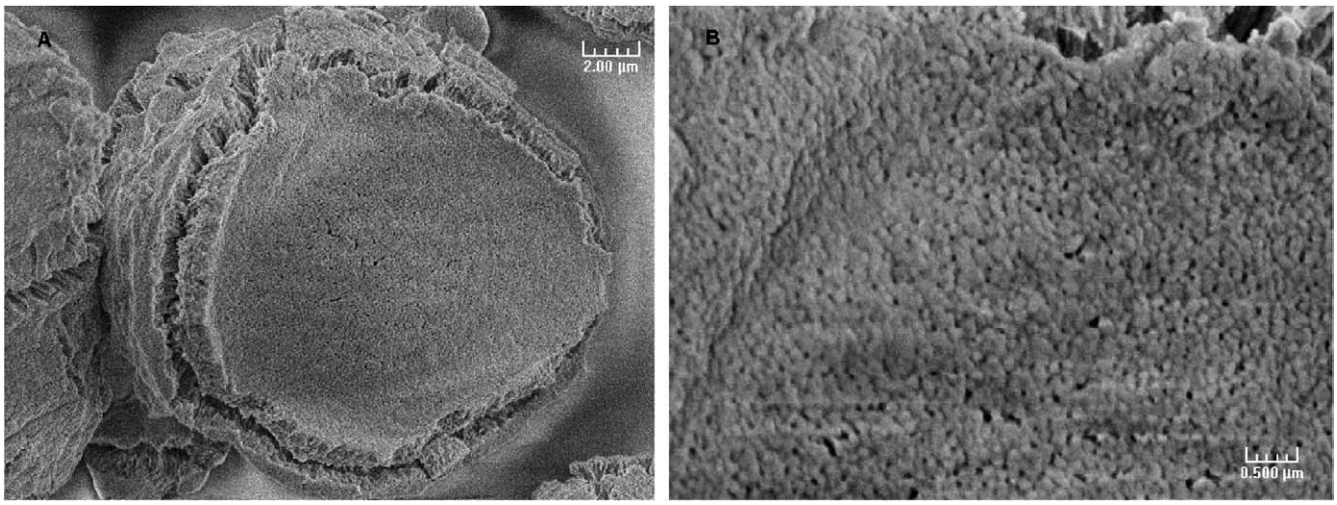

Fig. 4. SEM photographs of cross-sections of primary catalyst particles, collected at magnifications 5500× (A) and 30,000× (B).

ogy of Ti-based Ziegler–Natta catalysts prepared using other $MgCl_2$ crystallization methods, which usually exhibit a multigrain structure, with many very small (<1.5–2 μm) spherical particles of $MgCl_2$, loosely agglomerated in large secondary particles [17–19].

TEM observation of the catalyst is difficult; the rod-like crystallites are soft, and grinding the catalyst in a mortar (required to produce small fragments observable by the TEM method) results in strong shearing of the rod material. One example of a part of an undamaged rod is shown in Fig. 5. The rod diameter is ∼75 nm, in agreement with the SEM estimates. A layered lattice structure is observable in the rod; it is positioned mostly perpendicular to the rod length. TEM analysis under higher magnifications allows estimation of the lattice spacing in the crystalline rods, ∼5.8 A, which approximately corresponds to the distance between adjacent Cl–Mg–Cl layers, 1/3 of the elemental unit length in the *c* direction in the hexagonal $MgCl_2$ crystal. This crystal arrangement in the catalyst is very different from that in ball-milled Ti-based catalysts [20].

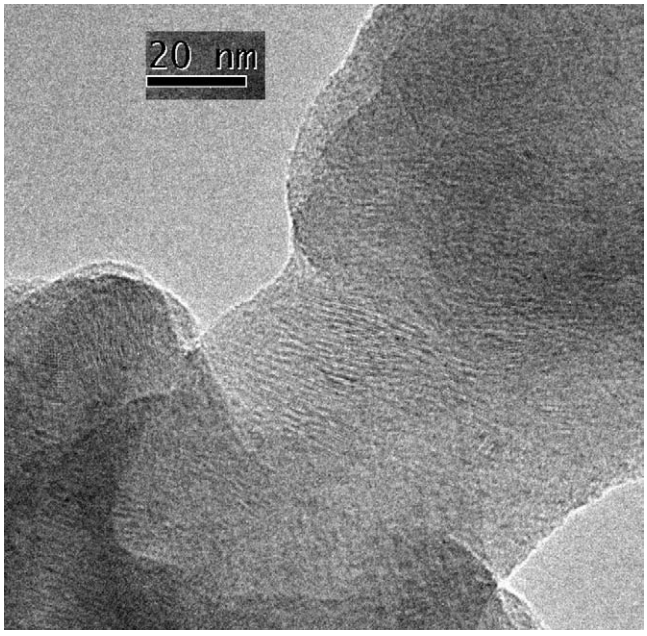

Fig. 5. TEM photograph of a section of the crystalline rod.

3.2. Crystalline structure

The XRD pattern of the catalyst is shown in Fig. 6. Three large peaks at $2\theta = 14.2°$, 16.8°, and 25.6° are due to polypropylene film, which is used to protect the catalyst from exposure to the atmosphere. Partial overlap of these peaks with some of the catalyst peaks does not interfere much with the data analysis. A comparison with the literature data on the crystal structure of different $MgCl_2$ modifications [20,21] leads to the following conclusions.

Two most common $MgCl_2$ modifications—cubic and hexagonal packing of the Cl–Mg–Cl layers—can be distinguished from the XRD pattern in the 2θ 30°–35° range. The cubic packing gives rise to two sharp reflections, (006) + ($10^{-}2$) at 30.4° and (104) at 35.2°, whereas the pattern of the hexagonal packing has three peaks, (002) at 30.6°, (101) at 32.4° (the strongest peak), and (002) at 35.2°. When $MgCl_2$ samples are subjected to ball-milling for a short period [20–27], the packing of the Cl–Mg–Cl layers becomes irregular, and the XRD pattern contains a very broad peak at ∼35° and a peak of a medium width at ∼30.5°. Prolonged milling results in merging of all peaks in the 28°–30° range into a single very broad peak with the maximum at ∼34° [27]. Based on the XRD modeling data [22,23,27], this pattern is due to the presence of Cl–Mg–Cl layers stacked along the *c* axis of $MgCl_2$ in a disordered manner.

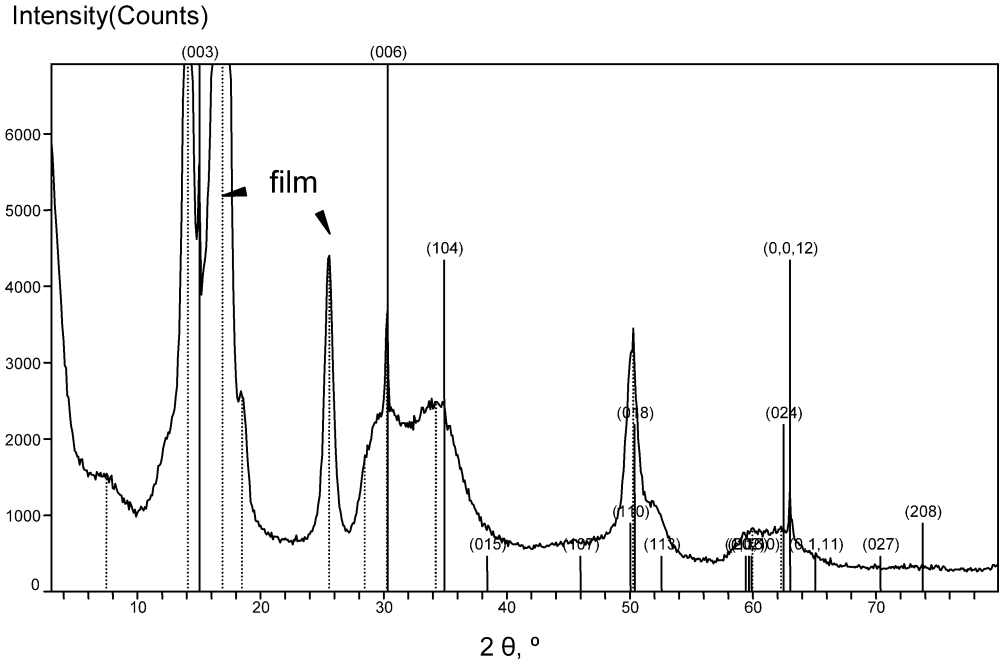

Fig. 6. Powder XRD pattern of the catalyst. Vertical lines give peak positions for hexagonal $MgCl_2$.

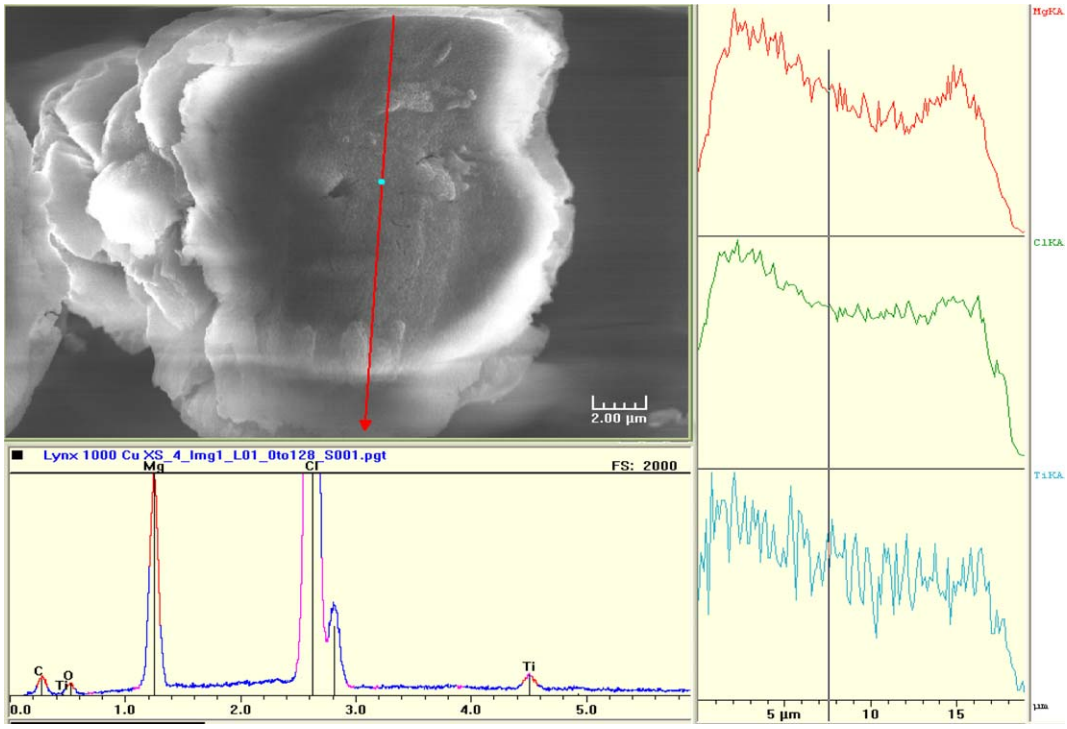

Fig. 7. SEM photograph of cross-section of a catalyst particle, collected at magnification 5000×, and the element distribution data. The arrow shows the direction of the EDS scan. Below the photograph is a typical EDS spectrum. The right-side curves are the element distributions along the line (top to bottom): Mg, Cl, and Ti.

Although the peak positions in the XRD pattern in Fig. 6 are similar to those of mildly ground $MgCl_2$, they differ strongly in their peak width, suggesting different morphologies of $MgCl_2$ crystals in the catalyst. Reflections from the planes perpendicular to the *c* axis of the $MgCl_2$ lattice, such as reflections (003) at 15.03°, (006) at 30.33°, and (0 0 12) at 63.01° (see Fig. 6), are relatively narrow, indicating that the number of the Cl–Mg–Cl layers in the stack is quite large. The reflections from the lattice planes positioned at relatively large angles to the *c* axis direction, such as the reflection from the (018) plane at 50.4°, have a medium width, and the reflections from the planes at sharp angles to the stack thickness, such as (104) at 34.92°, (110) at 50.02°, (113) at 52.58°, and (1 0 10) at 59.9°, are quite broad. This variation in width of different reflections is consistent with the morphology of the elemental motifs in the catalyst determined by the microscopic methods: relatively long and thin rods of $MgCl_2$ crystals containing stacks of Cl–Mg–Cl layers (Figs. 2–4).

An approximate estimation of the $MgCl_2$ crystallite width in the catalyst can be made from the line width at the half-heights of the broadest peaks in the XRD pattern. One such reflection is (104), which corresponds to the plane positioned at a relatively oblique angle to the plane of the Cl–Mg–Cl layers. A strong overlap of this peak with the $(10^{-}2)$ peak makes this estimation semiquantitative. The width at the half-height of the (104) peak, $\Delta(2\theta)$, is 3.4°–3.5°. Using the Sherrer formula, the average crystallite size in the lateral dimension is estimated to be ∼30–40 Å, a small value compared with the average width of the $MgCl_2$ rods (500–1000 Å).

3.3. Element distribution in catalyst particles

The distributions of three elements in the catalyst (Cl, Mg, and Ti) were analyzed using EDS on the SEM microscope. The inorganic constituents of the catalyst can be considered microcrystals of $MgCl_2$ with Ti compounds positioned on their surfaces. Chlorine atoms constitute the largest component of the catalyst (56.5 wt%), and the intensity of the Cl EDS peak can be used as a measure of the effective density of the catalyst particles (which are highly porous, as described above). Because of the low Ti content in the catalyst (∼5% of that of the Mg atoms), only a semiquantitative evaluation of the Ti distribution within the catalyst particles is possible.

Fig. 7 shows one example of the element distribution in the cross-section of a catalyst particle. Judging by the Cl distribution data, most catalyst particles have a nearly uniform apparent density with no large voids in the particles' centers. The distribution of Mg atoms follows the distribution of the Cl atoms, as expected for $MgCl_2$ crystals. The distribution of Ti atoms, in semiquantitative terms, also follows the distributions of Cl and Mg atoms. Ti atoms are distributed uniformly on the surfaces of the $MgCl_2$ crystals.

3.4. Growth model of catalyst particles

As described in Section 2, precipitation of solid $MgCl_2$ microcrystals occurs after the $MgCl_2$-containing solution is reacted with excess of $TiCl_4$ and the mixture is heated to 80 °C. Based on the SEM, TEM, and XRD data, the following model of the catalyst particle formation can be proposed.

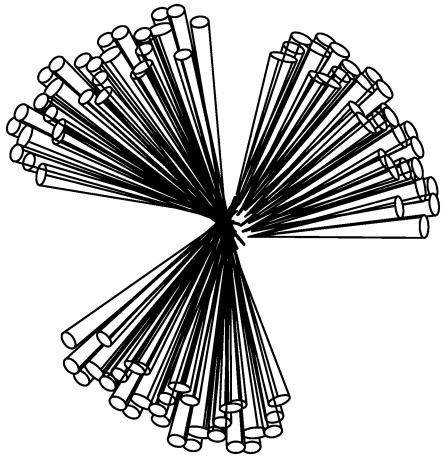

Fig. 8. The model of crystal growth resulting in formation of crystalline rods (compare to images in Fig. 3).

The growth of the $MgCl_2$ microcrystals starts at nucleation centers and progresses via the epitaxial crystal growth mechanism. Crystal growth can proceed in two perpendicular directions. The first of these is lateral expansion of the $MgCl_2$ motif (two layers of Cl ions with interstitial Mg ions in the six-fold coordination). Apparently, the extent of this growth is limited because of adsorption of $TiCl_4$ at exposed Mg atoms at the sides of the layered structure [24,25]. (In the next step of catalyst synthesis, the adsorbed $TiCl_4$ is partially replaced by diisobutyl phthalate.) According to the XRD estimation, the average size of the $MgCl_2$ crystallite in the lateral dimension is ∼30–40 Å, small compared with the average width of the $MgCl_2$ rods (500–1000 Å). It can be speculated that when the Cl–Mg–Cl sheets grow during the $MgCl_2$ crystallization, $TiCl_4$ molecules become adsorbed on the freshly formed lateral surfaces of the crystals. This adsorption does not completely interrupt the lateral growth of the $MgCl_2$ crystals, but it does limit the lateral size of $MgCl_2$ crystals to about 0.1–0.05 of the diameter of the $MgCl_2$ rods.

The second growth direction of the $MgCl_2$ crystals is predominant: stacking of the layered $MgCl_2$ motifs, resulting in the formation of quite long crystal rods with the Cl–Mg–Cl layers oriented perpendicular to the lengths of the rods and development of the sea urchin-type morphology evident from photographs in Figs. 3 and 4. This model of the crystal growth is shown in Fig. 8. Taking into account the area occupied by a single $MgCl_2$ moiety in the plane of the $MgCl_2$ motif, (∼10 $Å^2$), the cross-section of a typical crystal rod (∼5×10^5 $Å^2$) corresponds to 5×10^4 Mg atoms. It is equivalent to a circle of $MgCl_2$ moieties containing 250–300 Mg atoms across. The lengths of the crystalline rods are incomparably larger and, at a maximum, can reach the length of the radius of the primary particles. Growing primary $MgCl_2$ particles fuse at their surfaces, resulting in the formation of tight agglomerates, the final catalyst particles (Fig. 1).

An important question related to the morphology of the catalyst is the role of the dialkyl phthalate. Based on several semiquantitative data analyses on the distribution of O and C atoms in cross-sections of the catalyst particles, the phthalate molecules are adsorbed predominantly on the lateral surfaces of the $MgCl_2$ crystal rods, preventing the rods from fusing through lateral cocrystallization.

4. Conclusion

The article describes peculiar morphology of the $MgCl_2$-based support for a $TiCl_4/MgCl_2$-type Ziegler–Natta catalyst of the fourth generation. The support is prepared by forming toluene-soluble complexes of $MgCl_2$ with epichlorohydrin and tributyl phosphate at an increased temperature, followed by removing the organic components from the dissolved complexes with excess $TiCl_4$ at −25 °C. Heating this mixture results in precipitation of spherical $MgCl_2$-based particles with a unique sea urchin-type crystallite morphology.

Microscopic analysis shows that each particle of the support is an agglomerate of several spherical primary particles 5–8 μm in diameter. The primary particles are tightly filled with long rods of $MgCl_2$ crystallites. These rods radiate from the centers of the primary particles and are quite long; at a maximum, they can span the length of the radius of the primary particles. Within the rods, the planes of the Cl–Mg–Cl crystal layers are oriented mainly perpendicular to the lengths of the rods; that is, the *c* axis of the $MgCl_2$ crystals is parallel to the rod length. This arrangement of $MgCl_2$ crystallites exposes lateral surfaces of the $MgCl_2$ crystals, the surfaces on which the active sites of Ziegler–Natta catalysts are subsequently formed after treatment of the support particles with $TiCl_4$ [26].

References

[1] B.A. Krentsel, Y.V. Kissin, V.I. Kleiner, L.L. Stotskaya, Polymers and Copolymers of Higher α-Olefins, Hanser, Munich, 1997, chap. 3.
[2] Z.-Y. Ye, L. Wang, L.-F. Feng, X.-P. Gu, H.-H. Chen, P.-Y. Zhang, J. Pan, S. Jiang, L.-X. Feng, J. Polym. Sci., Part A: Polym. Chem. 40 (2002) 3112.
[3] M. Ferraris, F. Rosati, S. Parodi, E. Giannetti, G. Motroni, E. Albizzati, US Patent 4,399,054 (1983).
[4] M. Fujita, M. Sakuma, M. Tachikawa, M. Kuzaki, M. Miyazaki, Eur. Patent Appl. 187,035 (1986).
[5] K.E. Mitchel, G.R. Hawley, D.W. Godbehere, US Patent 4,988,655 (1991).
[6] V.M. Frolov, V.I. Kleiner, B.A. Krentsel, R.G. Mardanov, K.A. Munshi, Makromol. Chem. 194 (1993) 2309.
[7] J.J.A. Dusseault, C.C. Hsu, J. Macromol. Sci.: Rev. Macromol. Chem. Phys. C 32 (1993) 103.
[8] M. Kohyama, C. Tagarashi, K. Fukui, Eur. Patent Appl. 172,961 (1986).
[9] L. Luciani, J. Seppälä, B. Lofgren, Prog. Polym. Sci. 13 (1988) 37.
[10] G.G. Arzoumanidis, N.M. Karayanis, Appl. Catal. 76 (1991) 221.
[11] G.G. Arzoumanidis, N.M. Karayanis, Stud. Surf. Sci. Catal. 56 (1990) 147.
[12] C.B. Yang, C.C. Hsu, Y.S. Park, H.F. Shurvell, Eur. Polym. J. 30 (1994) 205.
[13] P. Sobota, J. Utko, T. Lis, J. Organomet. Chem. 393 (1990) 349.
[14] M. Chang, in: M. Terano (Ed.), Current Achievements in Heterogeneous Olefin Polymerization Catalysts, Sankeisha, Nagoya, Japan, 2004, p. 50.
[15] M. Chang, Y.V. Kissin, X. Liu, 4th JAIST/JLPO Workshop on Heterogeneous Ziegler–Natta Catalysts, Sorrento, Italy, 2005.
[16] B. Mao, A. Yang, Y. Zheng, J. Yang, Z. Li, US Patent 4,861,847 (1989).
[17] M.S. Pimplapure, G. Weickert, Macromol. Rapid Commun. 26 (2005) 1294.
[18] V.P. Oleshko, P.A. Crozier, R.D. Cantrell, A.D. Westwood, Macromol. Rapid Commun. 22 (2001) 34.
[19] H. Mori, T. Higuchi, N. Otsuka, M. Terano, Macromol. Chem. Phys. 201 (2000) 2789.

[20] U. Giannini, Makromol. Chem. Suppl. 5 (1981) 216.
[21] C. Dumas, C.C. Hsu, J. Macromol. Sci. Rev. Macromol. Chem. Phys. C 24 (3) (1984) 355.
[22] P. Galli, P. Barbe, G. Guidetti, R. Zannetti, A. Martorana, A. Marigo, M. Bergozza, A. Fichera, Eur. Polym. J. 19 (1983) 19.
[23] R. Zannetti, C. Marega, A. Marigo, A. Martorana, J. Polym. Sci., Part B: Polym. Phys. Ed. 26 (1988) 2399.
[24] P.C. Barbe, G. Cecchin, L. Noristi, Adv. Polym. Sci. 81 (1987) 1.
[25] V. Busico, P. Corradini, in: R.P. Quirk (Ed.), Transition Metal Catalyzed Polymerizations. Ziegler–Natta and Metathesis Polymerization, Cambridge Univ. Press, New York, 1988, p. 71.
[26] E. Albizzati, U. Giannini, G. Collona, L. Noristi, L. Resconi, in: E.P. Moor (Ed.), Polypropylene Handbook, Hanser, Munich, 1996, p. 11, chap. 2.
[27] F. Auriemma, G. Talarico, P. Corradini, in: T. Sano, T. Uozumi, H. Nakatani, M. Terano (Eds.), Progress and Development of Catalytic Olefin Polymerization, Technology and Education Publishers, Tokyo, 2000, p. 7.